PHYSICAL REVIEW D VOLUME 36, NUMBER 11 1 DECEMBER 1987

Resonance determination by stabilized analytic continuation of theoretical data, and comparison with the moments method

S. Ciulli, F. Geniet, and G. Mennessier
Laboratoire de Physique Mathématique, Université des Sciences et Techniques du Languedoc, 34060 Montpellier, Cedex, France

T. D. Spearman
School of Mathematics, Trinity College, Dublin 2, Ireland
(Received 15 October 1986; revised manuscript received 1 June 1987)

The conventional methods used so far with QCD sum rules stem from the observation that $s_1 - s$ (s_1 being the position of the first resonance) can be written as the limit of the ratio of the nth- and $(n+1)$th-order moments, or are based on similar techniques such as those of Borel operators. Unfortunately, apart from the fact that practical instabilities appear because one uses high derivatives of very smooth functions, these methods do not have internal controls which would enable them to adapt to the varying precision of the theoretical information for different values of the energy in the spacelike region, to finite resonance widths, threshold behaviors, etc. There are alternative procedures, however, based on extremal problems and leading to simple (Fredholm) integral equations, which are flexible enough to accommodate these various practical requirements. Computer tests have been carried out, using these procedures, on a number of completely soluble quantum-mechanical examples, and the comparison with the conventional moments techniques is described.

I. CONVENTIONAL QCD SUM RULES

The interest in sum rules and related techniques of analytic extrapolation in QCD is due to the fact that in practice it is not possible to calculate directly the quantities of interest, such as amplitudes or form factors, for physical (timelike) energy values. It may however be possible to perform perturbative, or some specific nonperturbative calculations at spacelike points, and one is then tempted to turn to some method of analytic continuation to obtain physical information, such as the values of resonance parameters.

Typical of the methods so used is that based on moments. This was illustrated, in the context of a simple model, by Bell and Bertlmann.[1] The central idea is that the ratio $r_n(Q^2) \equiv M_n(Q^2)/M_{n+1}(Q^2)$ gives, in the large-n limit,

$$\lim_{n\to\infty} [r_n(Q^2) - Q^2] = s_1 \ , \tag{1}$$

where s_1 is the position of the first resonance. The notation here is that $Q^2 \equiv -s$ is positive, and the "moment" $M_n(Q^2)$ is defined as

$$M_n(Q^2) \equiv \frac{1}{(n-1)!} \frac{d^{n-1} A(s)}{ds^{n-1}} \bigg|_{s=-Q^2} . \tag{2}$$

This result has been examined in a recent paper by Bowcock, Ciulli, and Geniet.[2] There it is shown that whereas Eq. (1) is valid when there is no right-hand cut, that is, when $A(s)$ has no imaginary part on the real axis and the "resonance" poles are located on the real axis, the situation changes when a cut is introduced. In that case, the limit in Eq. (1) does not yield s_1 but s_0, the lowest branch point. As shown in Ref. 2 this comment concerns not only the Bell and Bertlmann method, but also the so-called "Borel operator" one. This is easy to understand since, as shown for instance by Reinders, Rubinstein, and Yazaki,[3] the Borel method can be deduced from the Bell and Bertlmann one. So we shall focus our attention on the behavior of the moments.

To illustrate this it is helpful to look at a simple soluble quantum-mechanical example. Consider the Green's function for the one-dimensional potential $V(x) = v_0[\delta(x - 1/2m) + \delta(x + 1/2m)]$. The parameters have been chosen so that the first two resonances of the Green's function will have their corresponding second-sheet poles at suitable values of E. (In particular, when $v_0 = 10$, $E_1 = 4.1 \pm 0.1i$, $E_2 = 37.8 \pm 2.3i$, . . . , and when $v_0 = 3$, $E_1 = 2.9 \pm 0.5i$, $E_2 = 32.2 \pm 7.8i$, . . . , all in units of m; for this nonrelativistic example we have used the energy variable E instead of s.) The results from applying the moments method to this example, for $v_0 = 10$ and 3, are shown in Fig. 1. In each case the integral over the branch cut, say from E_0 to $\mathrm{Re}E_1$, is small[4] compared with the contribution from the resonance poles at $E = E_1$, E_1^*. In Fig. 1 (see the discussion in Ref. 2), the graph of $r_n - Q^2$ against n, for $v_0 = 10$, shows a brief inflection at $r_n - Q^2 \approx \mathrm{Re}E_1$ for values of n in the range 3–10. For larger n it moves towards the asymptotic value which is E_0. In a case such as this, the moments method can be used to give an approximate value of E_1 by identifying the inflection mentioned above. Such an inflection will, however, only appear when the integral over the branch cut is very small compared with the contribution from the resonance. In the graph corresponding to $v_0 = 3$ it is much less pronounced, although the cut contribution is again small.

In Fig. 2 one treats the form-factor case[5] where the integral over the cut is more nearly comparable to the res-

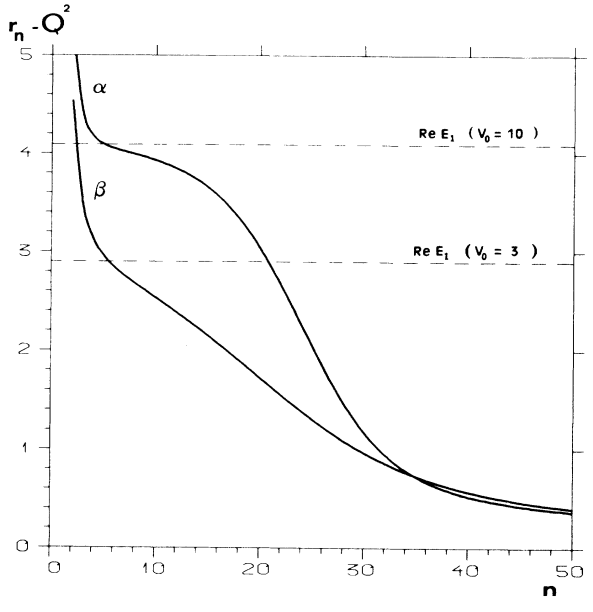

FIG. 1. Plots of $r_n - Q^2$ against n for the one-dimensional quantum-mechanical Green's function for (α) $v_0 = 10$ and (β) $v_0 = 3$. The dashed line in each case is $r_n - Q^2 = \mathrm{Re}E_1$. The common large-$n$ asymptote for both graphs for $r_n - Q^2$ is equal to the threshold value of the energy which is 0.

onance contribution;[5] in this case there is no perceptible inflection. In any event, an inflection will only be observed if the precision of the input data, used to evaluate M_n, is very high. The alternative method, which will be described in the next section, can readily distinguish between the effect of a cut with slowly changing discontinuity, and an effect with a rapidly changing imaginary part such as that associated with a narrow resonance.

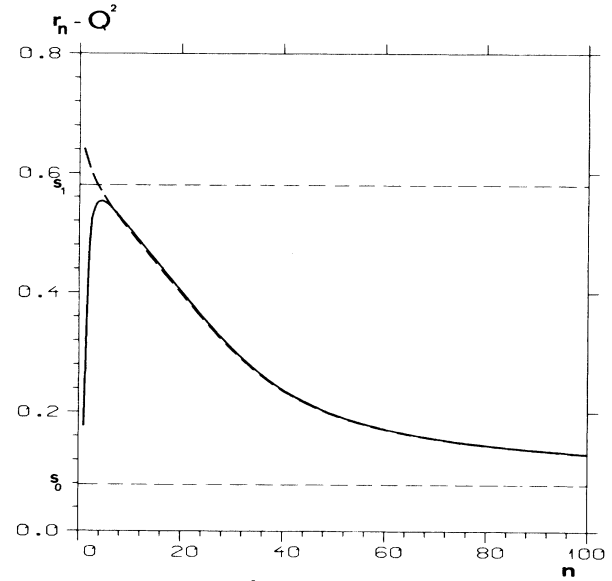

FIG. 2. Plot of $r_n - Q^2$ against n for the form factor $\Pi(s)$. The solid line corresponds to the Heyn and Lang function, the dashed line to the same function without corrective terms. The thin dashed lines are $r_n - Q^2 = s_1$ and $r_n - Q^2 = s_0$, the resonance and threshold positions, respectively.

II. ALTERNATIVE METHOD USING STABILIZED ANALYTIC CONTINUATION

The main practical problem one has with analytic continuation is that even if one starts with two almost identical functions in the data region, one may end up with results differing arbitrarily much in other points of interest (e.g., in the resonance region on the cuts). To cope with this situation one has to stabilize the analytic continuation by means of conditions which should filter out the spurious results. These conditions will be expressed in terms of norms. As the basic principles underlying this approach have already been described in some detail[6] we shall just summarize the results here. The s plane is first mapped onto the unit disk. The map of the data region $s < 0$ ($Q^2 \equiv -s > 0$) is on the real axis $|z| < 1$, and we restrict this to some range γ. The right-hand cut in the s plane, commencing at $s = s_0$, maps onto the circle $z = e^{i\phi}$, with $s = s_0 \to \phi = 0$. The second-sheet poles $s = s_1 \pm iK_1$, $s_2 \pm iK_2, \ldots$, map to conjugate pairs of points which lie outside the circle at, say, z_1, z_1^*, and z_2, $z_2^*, \ldots$. The problem to be solved is to use approximate data on γ to obtain information about the positions and residues of these poles. The approach to this problem which we wish to describe is based on the definition of a suitable norm[6] on the space of functions $X(z)$ which are holomorphic in $|z| < 1$. This norm is defined in terms of the boundary values on the circle $z = e^{i\phi}$.

There are two key aspects to defining this norm: (i) the need to be sensitive to a rapidly changing imaginary part such as that associated with a narrow resonance and (ii) the use of a real positive weight function which permits a different weighting on different parts of the circle (i.e., of the cut $s_0 \le s < \infty$), and which also allows one to impose particular forms of threshold behavior (at $s = s_0$, or asymptotic behavior at $s \sim \infty$). The use of $\sigma(\phi)$ to impose threshold behavior is discussed in Sec. III.

A particularly useful form of the norm is (the Neumann norm, see Ref. 6)

$$\|X\|^2 = \frac{1}{2\pi} \int_0^{2\pi} [x_r(\phi)]^2 \sigma(\phi) d\phi \ , \tag{3}$$

where

$$x_r(\phi) = \frac{\partial \,\mathrm{Re}X(re^{i\phi})}{\partial r}\bigg|_{r=1} = \frac{\partial \,\mathrm{Im}X(e^{i\phi})}{\partial \phi} \ . \tag{4}$$

This norm has been chosen to be particularly sensitive to a rapidly changing imaginary part, such as that associated with a narrow resonance. Note that $\|X\|$ does not define a norm on the whole space of functions, but only on a subspace for which the value of $X(z)$ at some point, say z_0, is fixed. If we put $X(z_0) = d_0$, then the function $X(z)$ is given in terms of

$$x_r(\phi) \equiv \frac{\partial \,\mathrm{Im}X(e^{i\phi})}{\partial \phi}$$

by

$$X(z) = d_0 + \frac{1}{\pi} \int_0^{2\pi} \ln \frac{e^{i\phi} - z_0}{e^{i\phi} - z} x_r(\phi) d\phi \ . \tag{5}$$

The reader will observe that, in contradistinction to oth-

er methods using analytical weights, the weight σ does not here enter the relation between the boundary function $x_r(\phi)$ and $X(z)$ inside the analytic domain [in the "dispersion relation" (5)]. (Analytic weights may, for instance, blow up in other parts of the holomorphy domain.) In the present method σ enters only the norm (3) defined on the cuts and, of course, may be nonanalytic. Incidentally, all results obtained in this paper could be found almost identically using a constant function $\sigma(\phi)$, apart from the threshold behavior discussed in Sec. III.

Suppose now that we are interested in an amplitude $A(z)$, for which we are given data $a(z_\gamma)$ on the set γ, say for $-\alpha<z<\alpha$. We wish to ask if the data provide evidence for a pair of conjugate second-sheet poles corresponding to a resonance. What we do is to construct a function $T_k(z)$ which corresponds precisely to such a pair of poles with parameter values indicated by k ($k\equiv\{k_1,k_2,\ldots\}$). We then construct the so-called discrepancy function $D_k(z)$:

$$d_k(z)\equiv a(z)-T_k(z),\quad d_k(z)\equiv a(z)-T_k(z)\ . \tag{6}$$

If the amplitude $A(z)$ has a resonance, and if the parameter values k are correctly chosen, then $D_k(z)$ will have a smaller norm than $A(z)$, or than it would have had if the parameters had been chosen incorrectly. This will be particularly the case if one uses a suitably chosen "window"[6] inside which $\sigma(\phi)$ is large.[6] So the idea is to evaluate $\|D_k\|$ for different values of the parameter set k and to look for a minimum, which should then correspond to the values of the resonance parameters.

Initially neither $A(z)$ nor $D_k(z)$ is known outside γ. To make the continuation from the data $d_k(z_\gamma)$ on γ, to $D_k(z)$ in $|z|<1$, some stabilizing procedure is needed; this is provided by requiring that $\|D_k\|$ should have a minimum value, subject to an adequate fit to the data $d_k(z_\gamma)$ as specified by an appropriate value of χ^2, say $\chi^2=1$. The problem is now expressed in terms of two functionals:

$$F_1[x_r]\equiv\delta^2[D_k]=\frac{1}{2\pi}\int_0^{2\pi}[x_r(\phi)]^2\sigma(\phi)d\phi\ , \tag{7}$$

$$F_2[x_r]\equiv\chi^2[D_k]-1=\int_\gamma dz\,n(z)\left[d_k(z)-d_0-\frac{1}{2\pi}\int_0^{2\pi}N(z_0;z,e^{i\phi})x_r(\phi)d\phi\right]^2-1\ , \tag{8}$$

where $n(z)\equiv[\epsilon(z)]^{-2}$, $\epsilon(z)$ being the error associated with the data $d_k(z)$ on γ; $d_0\equiv D_k(z_0)$; $x_r(\phi)\equiv(\partial/\partial\phi)\mathrm{Im}D_k(e^{i\phi})$; and the Neumann kernel $N(z_0;z,e^{i\phi})$ is

$$N(z_0;z,e^{i\phi})\equiv 2\ln|(e^{i\phi}-z_0)/(e^{i\phi}-z)|\ . \tag{9}$$

$F_1[x_r]$ is to be minimized subject to the condition that $F_2[x_r]=0$. In terms of a Lagrange multiplier λ, this requires that $\delta F[x_r]=0$, where $F\equiv F_1+\lambda F_2$. The minimization is with respect to both d_0 and the function $x_r(\phi)$: this yields an optimized function $x_r^0(\phi)$ as the solution to a Fredholm integral equation which has the form

$$x_r^0(\phi)\sigma(\phi)=\lambda G_k(\phi)+\lambda\frac{1}{2\pi}\int_0^{2\pi}d\phi' K(\phi,\phi')x_r^0(\phi')\ , \tag{10}$$

where

$$G_k(\phi)\equiv\int_\gamma dz\,n(z)N(z_0;z,e^{i\phi})\times\left[d_k(z)-\frac{1}{n_\gamma}\int_\gamma dz'n(z')d_k(z')\right]\ , \tag{11}$$

$$K(\phi,\phi')\equiv\frac{1}{n_\gamma}\int_\gamma dz\,n(z)N(z_0;z,e^{i\phi})\times\int_\gamma dz'n(z')N(z_0;z',e^{i\phi'})-\int_\gamma dz\,n(z)N(z_0;z,e^{i\phi})N(z_0;z,e^{i\phi'})\ , \tag{12}$$

and

$$n_\gamma\equiv\int_\gamma n(z)dz\ .$$

The solution for d_0 is given in terms of $x_r^0(\phi)$, λ is chosen to satisfy the condition that $F_2[x_r]=0$ (i.e., $\chi^2=1$), and finally we obtain the optimized function $D_k^0(z)$ as

$$D_k^0(z)=d_0+\frac{1}{\pi}\int_0^{2\pi}\ln\left[\frac{e^{i\phi}-z_0}{e^{i\phi}-z}\right]x_r^0(\phi)d\phi\ , \tag{13}$$

where

$$d_0=\frac{1}{n_\gamma}\int_\gamma dz\,n(z)d_k(z)-\frac{1}{n_\gamma}\int_\gamma dz\,n(z)\left[\frac{1}{2\pi}\int_0^{2\pi}d\phi\,N(z_0;z;e^{i\phi})x_r^0(\phi)\right]\ .$$

This is repeated for different sets of k values; in each case the norm $\delta_0{}^2\equiv\|D_k^0(z)\|$ is evaluated, and the values of the parameter set k for which $\delta_0{}^2$ has a minimum value are determined.

III. THE INCORPORATION OF THRESHOLD BEHAVIOR AND SUBTRACTION CONSTANT

In applying the method described in Sec. II it is important to be able to incorporate such special features as a subtraction condition or a threshold behavior in an amplitude or form factor. To illustrate how to do this

we consider, as a particular example which is of interest, the pion form factor $\Pi(s)$. In this case, we must impose two conditions on the functions $X(z)$ as follows:

$$\text{(i)}\quad X(z_0)=d_1$$

and (14)

$$\text{(ii)}\quad x_r(\phi)\equiv\frac{\partial\,\mathrm{Im}X(e^{i\phi})}{\partial\phi}\sim\phi^2 \text{ for small } \phi\text{'s} .$$

Here the point z_0 is the interior point of the circle, $|z_0|<1$, which corresponds to $s=0$. Since $X(s)=\Pi(s)-T_k(s)$, by choosing the test function $T_k(s)$ to be zero at $s=0$, we get $d_1=\Pi(s=0)=1$. The condition on $x_r(\phi)$ applies at $z=1$, corresponding to the threshold $s=s_0$, and comes from the condition that $\mathrm{Im}X(r)\sim(1-z)^3$ near $z=1$.

A. Fixed subtraction equation

The first point to note is that the point z_0 in (14) may be identified with the subtraction point z_0 in Sec. II which sets the constant $d_0=d_1$. This simplifies the problem considerably in that d_0 is now fixed in Eq. (8) and the minimization $F[x_r]=0$ is now with respect to x_r alone. The form of the integral equation (10) is exactly as before:

$$x_r(\phi)\sigma(\phi)=\lambda G_k(\phi)+\lambda\frac{1}{2\pi}\int_0^{2\pi}d\phi' K(\phi,\phi')x_r(\phi') , \quad (10)$$

but $G_k(\phi)$ and $K(\phi,\phi')$ are now given by

$$G_k(\phi)\equiv\int_\gamma[d_k(z)-d_1]n(z)N(z_0;z,e^{i\phi})dz , \quad (15)$$

$$K(\phi,\phi')\equiv-\int_\gamma n(z)N(z_0;z,e^{i\phi})N(z_0;z,e^{i\phi'})dz , \quad (16)$$

which are rather simpler expressions than those of Eqs. (11) and (12) for the case when d_0 is also varied.

B. σ weight and threshold behavior

At this stage the condition $X(z_0)=0$ has been imposed, but not $x_r(\phi)\sim\phi^2$. To introduce the latter condition one must, in effect, reduce the space of functions x_r, to those with behavior $\sim\phi^2$. In order to confine the extremum problem to this restricted space, it is necessary to use an appropriately defined norm $\|X\|$ using the flexibility provided by the weight function $\sigma(\phi)$. From the norm definition (3) one might suppose that $\sigma(\phi)$ should be given the form ϕ^{-4}, to ensure a ϕ^2 behavior for $x_r(\phi)$. In fact this would be too strong a constraint. Although the minimization would take place within the space of functions $x_r\sim\phi^2$, the result of that process would have the behavior $x_r^0\sim\phi^4$. This is evident from the integral equation (10), with $G_k(\phi)$ and $K(\phi,\phi')$ given by Eqs. (15) and (16). One sees at once that to make $\sigma(\phi)\sim\phi^{-2}$ is a sufficient condition to ensure that the solution $x_r^0(\phi)$ to the minimization problem is $\sim\phi^2$.

It is clear that the reasoning used above is applicable to a variety of different threshold or asymptotic conditions. For example, one might wish to treat an elastic p-wave scattering amplitude for which $X(z=1)\sim k^2\sim(1-z)^2$, with the stronger condition on the imaginary part that $\mathrm{Im}X(z=1)\sim(1-z)^5$ giving $x_r(\phi)\sim\phi^4$. In this case the point $z=z_0$ for which $X(z)=0$ becomes $z=1$ while the vanishing of $X'(z=1)$ is resolved by means of an additional Lagrange multiplier; these question will be discussed in more detail elsewhere. Replacing z_0 by 1 introduces logarithmic factors in $N(1;z,e^{i\phi})$ which must be compensated for in $\sigma(\phi)$ to give the required behavior to $x_r(\phi)$. It is easily verfied that $\sigma\sim\phi^{-4}\ln\phi$ gives the desired result.

There is one point about the effect of incorporating a zero, whether at the threshold $z=1$ or at an interior point z_0 with $|z_0|<1$, which is of practical importance and so merits mention. When one carries out the minimization described in Sec. II, the variation with respect to d_0 alone can achieve a substantial reduction in χ^2 or $\delta_0{}^2$ without minimizing over x_r. This reduces the predictive power of the minimization process with respect to $x_r(\phi)$. On the contrary when the amplitude has an exactly known value at one point[7] which can be used to replace d_0 in the way described above, the minimization is focused on $x_r(\phi)$ alone. As will be seen from the numerical example discussed in the next section (Fig. 6), the corresponding curve has a sharper minimum.

IV. COMPARISON OF THE TWO METHODS: NUMERICAL RESULTS

To compare the effectiveness of the two methods, the one based on moments, the other using stabilized analytic continuation as described in Sec. II, we show the results of applying each method to two simple models. The first of these is the one-dimensional quantum-mechanical model described in Sec. I, looking at the Green's function for the potential

$$V(x)=v_0\left[\delta\left[x-\frac{1}{2m}\right]+\delta\left[x+\frac{1}{2m}\right]\right] . \quad (17)$$

The first resonance, which we wish to locate, corresponds to second-sheet poles at $E_1=4.1\pm0.1i$ when $v_0=10$, and at $E_1=2.9\pm0.5i$ when $v_0=3$, all in units of m. The Green's function has in each case a cut extending from the threshold, $E_0=0$, to $+\infty$. The results of the moments calculation are shown in Fig. 1. As was pointed out in Sec. I for $v_0=10$ there is a perceptible inflection at $E\approx E_1$ for values of n in an approximate range 3–10, and this does allow the possibility of estimating the value of E_1; however, for $v_0=3$ the inflection is much less pronounced. In these calculations the moments were evaluated at $E=-10$. Figures 3(a) and 3(b) show the result obtained using the method of stabilized analytic continuation. In this case the data input is taken over the range -1 to -50 for E. The two curves shown in each of Figs. 3(a) and 3(b) correspond to different error assignments for the data $a(z)$. $\delta_0{}^2$ is plotted against the real part of the pole position in the trial function, and in each case there is a clear minimum yielding a reasonable value for $\mathrm{Re}E_1$, the real part of the pole position. In this particular calculation the other parameters (the imaginary part of the pole position and the residue) have been held fixed at reasonable values, but a more careful calculation in which these are varied

simultaneously yields essentially similar results.[8] As the errors assigned to the data are increased, so the precision of the resonance determination is reduced; this must be the case. The threshold, as expected, does not manifest itself.

It is informative to combine the results of the two methods in one diagram. This has been done in Figs. 4(a) and 4(b) for the Green's-function example. These diagrams are simply the superposition of graphs taken from Fig. 3 and from Fig. 1 (with the x and y axes interchanged for the Fig. 1 graphs, and taking the ρ_2 graph from Fig. 3).

The second model is related to the pion form factor $\Pi(s)$ and is based on the parametrization of Heyn and Lang[9] which is known to be in good agreement with the recent experimental data.[10] We have used the solution A of Ref. 9 which seems to be in better agreement with the far spacelike data predicted by QCD. We would not like to argue here about the best choice between the different solutions of Heyn and Lang, but we have used here their spacelike data only as a test for the predictive power of our integral equations in the timelike region.

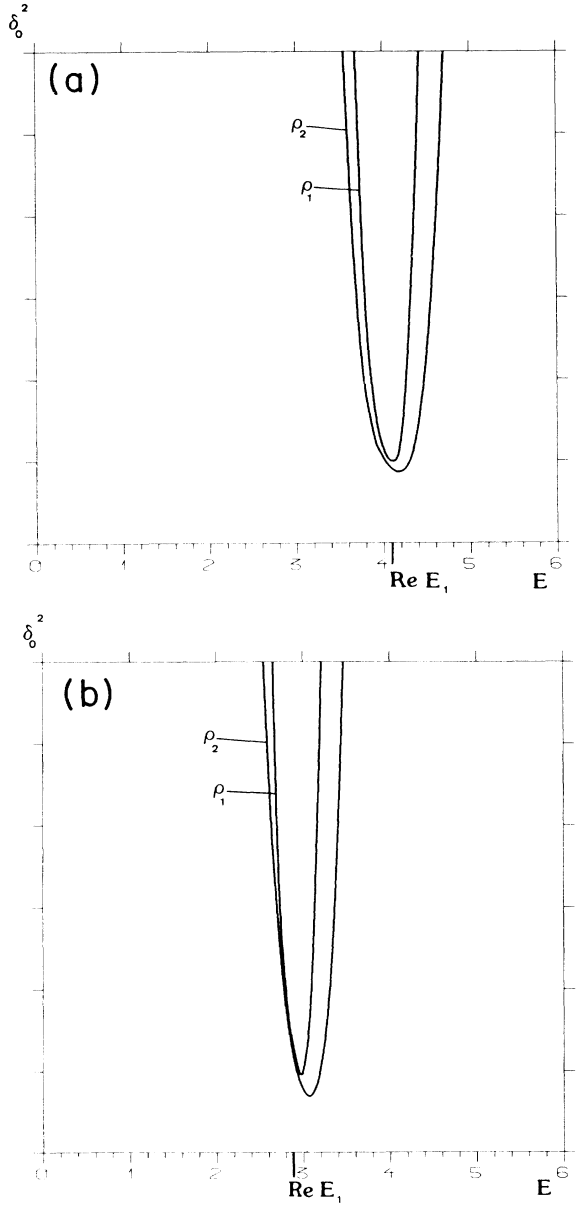

FIG. 3. δ_0^2 plotted against the real part of the pole position for the Green's function for the quantum-mechanical example, with (a) $v_0=10$ and (b) $v_0=3$. The two curves, in each case, correspond to different errors assigned to the data: these are 1 part in 5×10^4 (ρ_1) and 1 part in 10^4 (ρ_2).

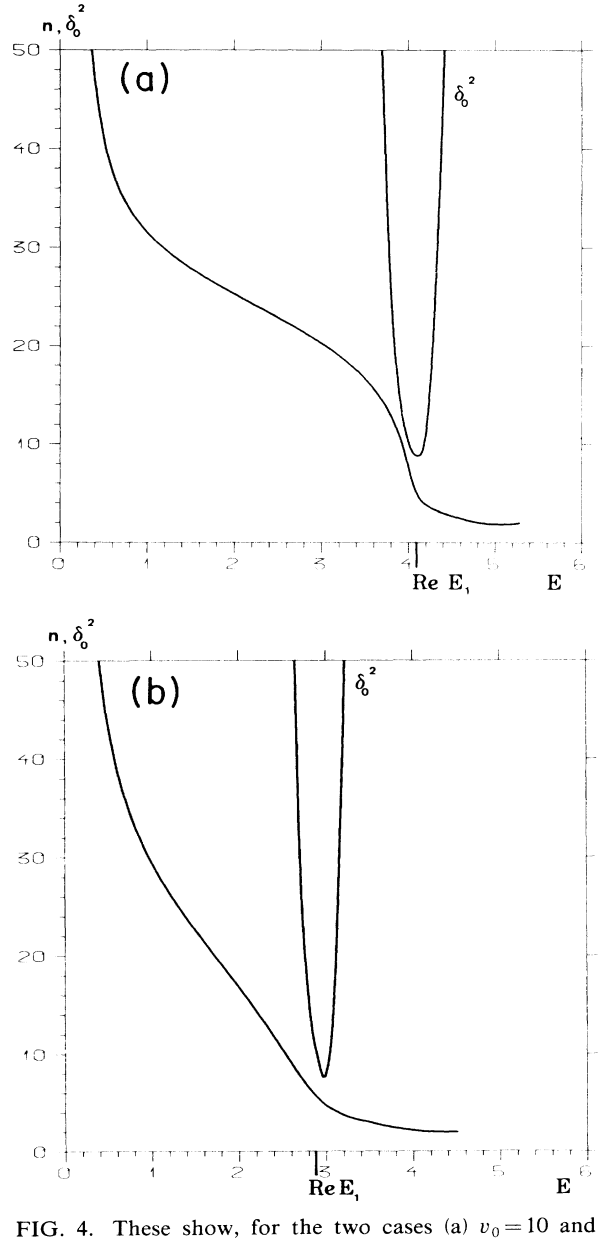

FIG. 4. These show, for the two cases (a) $v_0=10$ and (b) $v_0=3$ the effect of superimposing the graphs from Figs. 1 and 3. The n axis has been chosen to be vertical to facilitate the comparison. E_1 is the resonance pole position ($\mathrm{Re}E_1=4.09$ and 2.9, respectively). δ_0^2 is shown in terms of units based on its minimum value.

The moments M_n were evaluated at $s \equiv -Q^2 = -2$ GeV^2. In order to compute exactly the high derivatives entering the moments M_n we have used a dispersion relation over the imaginary part of the Heyn and Lang solution. The same procedure has been used also to check the Borel method. The result of the moment calculation is shown in Fig. 2. There is no inflection around the value s_1, but interesting enough, the curve grows for the first three moments up to a maximum, which happens to lie at the position of the resonance, before tending as it should to the threshold value. We were surprised to see this maximum but, since it did not appear in any previous computations, we suspected that it was related to an instability rather than to the resonance itself. (One should, of course, bear in mind that the theorems concerning moments apply to the high-n limit and *not* to small values of n.) If that were the case then the maximum should be sensitive to small variations in the input function. To check this, we repeated the computation using the Heyn and Lang function without their small corrective parameters. Although the resonance in the timelike region was almost unaffected by this change, the maximum from the moments curve disappeared completely (see the dashed curve in Fig. 2). This shows that this effect has been just a fluctuation because of the lack of stability of the procedure for small-n values. This occurrence demonstrates the importance of having stable procedures.

Figures 5 and 6 show the results obtained using the methods of Secs. II and III, respectively. In these calculations the data obtained by evaluating Eqs. (18) and (19) were taken in the range -0.5 to -50 for s.

The two curves in Fig. 5 correspond to two different error assignments and each shows $\delta_0{}^2$ plotted against the real part of the position s_1 in the trial function. In this case, no particular threshold behavior at $s = s_0$ was imposed on $\Pi(s)$, nor the constant at $s = 0$. Despite the rather crude nature of the calculation, the result is quite good and yields a reasonable value for $\mathrm{Re}s_1$. Here again, the minimization of $\delta_0{}^2$ with respect to the pole parameters was limited to $\mathrm{Re}s_1$; the residue and $\mathrm{Im}s_1$ were held fixed at reasonable values.

A more sophisticated, and more reliable, analytic continuation would use the results of Sec. III taking account of the constraint at $s = 0$ and the threshold behavior at $s = s_0$. The results of such a calculation are shown in Fig. 6. The solid line shows the plot of $\delta_0{}^2$ against the real part of the pole position in the trial function for the form factor. Following the procedure described in Sec. III, $\Pi(s)$ was, in this case, constrained to have the value 1 at $s = 0$, and to have the threshold behavior $\mathrm{Im}\Pi(s) \sim (s - s_0)^{3/2}$. The weight function $\sigma(\phi)$ was given the form $\sigma \sim \phi^{-2}$ at $\phi = 0$ in order to impose this threshold behavior to the derivative of the imaginary part. The trial functions T_k were constructed[11] so as to satisfy the same constraints as were imposed on Π.

For comparison we have plotted here (Fig. 6) also (a) the results of Fig. 5 where no subtraction nor threshold condition were imposed at all (the dashed line), as well as (b) the curve obtained when the threshold behavior has been imposed using the above $\sigma(\phi) \sim \phi^{-2}$ form, but

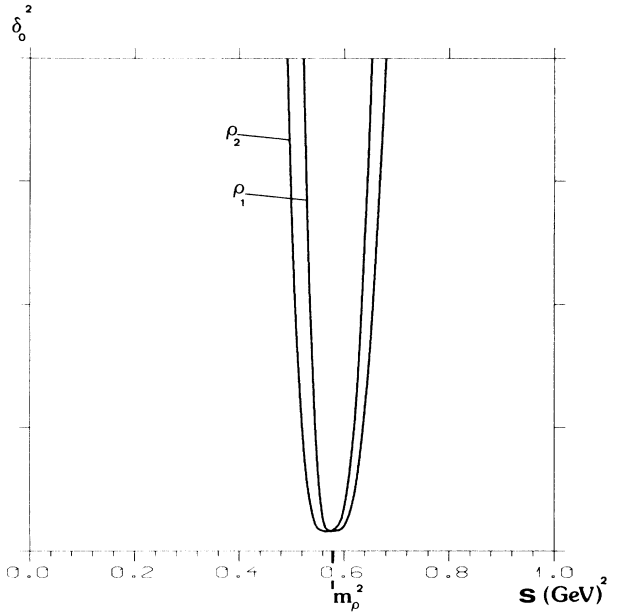

FIG. 5. $\delta_0{}^2$ plotted against the real part of the pole position for the form factor [Eqs. (18) and (19)]. The two curves correspond to the assignation of different errors: ρ_1 is 1 part in 1×10^4, ρ_2 is 1 part in 5×10^3.

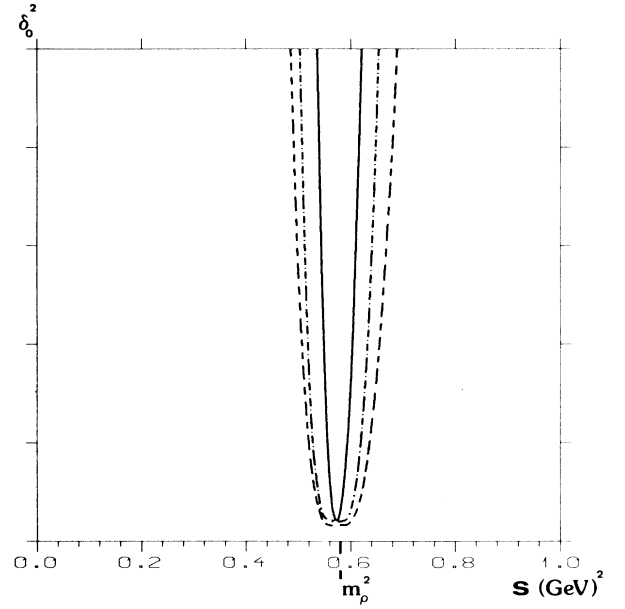

FIG. 6. Step by step improvement of the analytic continuation process in the form-factor case. The dashed line represents $\delta_0{}^2$ vs the real part of the pole position when no specific information has been added. [The integral equations (11) and (12) have been used with $\sigma = 1$.] The dashed-dotted line: same equations (11) and (12) but with a σ weight constraining the solution to have a correct threshold behavior $\mathrm{Im}\Pi(s) \sim (s - s_0)^{3/2}$. Solid line: the integral equations (15) and (16) have been used, when the threshold and the subtraction constant $\Pi(s = 0) = 1$ has been specified.

where $\Pi(s=0)$ has not yet been constrained to have the value 1 (the dashed-dotted line). One may hence see directly the improvement obtained by adding supplementary information and changing correspondingly the integral equation. One may notice that the minimum is much sharper with the solution of the Eqs. (15)–(16) using the constraint $\Pi=1$ at $s=0$, the reason being that the minimization with respect to d_0 is no longer carried out. As discussed in Sec. III this minimization would have given a substantial reduction of χ^2 and $\delta_0{}^2$ by itself, thus reducing the role of the function $x_r(\phi)$ and hence the predictive power of the method. It is interesting to note, however, that the value of $\delta_0{}^2$ at the point $\mathrm{Res}\approx 0.55$, which corresponds to the minimum of the solid curve, is almost the same for both graphs. One can deduce from this observation that the value of $\Pi(0)$ obtained by minimization of d_0, for *that* value of the trial pole position, should be close to 1, which is the imposed value for the solid curve. In fact that value obtained is 1.002.

In comparing the curves in Fig. 6 it is important to note that the norms are different because of the different forms of the weight function $\sigma(\phi)$. (The error factor ρ in Fig. 6 is 1 part in 5×10^3, this is the same as ρ_2 in Fig. 5.)

In Fig. 7 we have plotted (the dashed-dotted curve) the modulus squared of the form factor reconstructed—using the method described in Sec. II at timelike energies. The minimization of $\delta_0{}^2$ has been performed with respect to all the parameters entering in the pole trial function $T_k(s)$, that is, the pole position in the complex s plane and the residuum value.[12] Together with this dashed-dotted reconstructed function, Fig. 7 also shows "the true function" (the solid curve), i.e., the Heyn-Lang input function used to produce the data in the spacelike region. The agreement is remarkable. In particular one sees that a correct prediction for the width of the resonance has been obtained, together with a correct resonance position.

The solution obtained by this method ($\delta_0{}^2$ minimization) changes very little when the small Heyn and Lang correction terms, which modify the pure Breit-Wigner formula, are neglected (in contrast with the moments curve, Fig. 2, which is quite unstable to this small modification).

One question which might be asked is whether a direct χ^2 fit to the same spacelike data by the pole function $T_k(s)$ alone, without any of the relatively elaborate analysis described above, might yield reasonable results. We carried out such an exercise (using the same CERN MINUIT minimization routines as we had used to obtain the minimum of $\delta_0{}^2$) and the resulting function obtained in this way is shown as the dotted curve in Fig. 7. As can be seen the result is rather poor: the predicted energy of the resonance is too low, and the imaginary part of the pole position is small, yielding too narrow a resonance. We also found that this method [naive χ^2 fit for $T_k(s)$] is also quite unstable to small variations in the input data; for example, if the input data had been precisely the imaginary part of a Breit-Wigner formula (which would have been the case if the small correction terms of Heyn and Lang had not been included) then the result would have been exact and the dotted curve would have coincided with the input function, in contrast with the result displayed in Fig. 7.

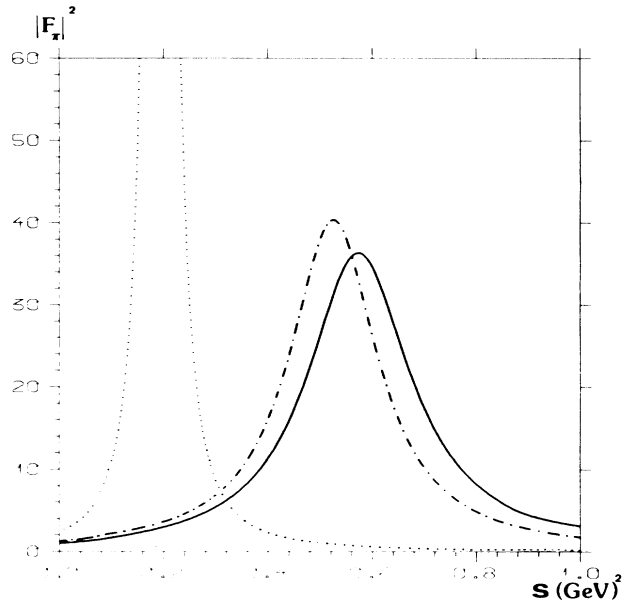

FIG. 7. $|F_\Pi|^2$ plotted against s, the energy squared in the c.m. frame. The solid line represents the function of Heyn and Lang. The dotted-dashed line is the solution of the integral equations (10). The dotted line represents a naive direct χ^2 fit of the spacelike data.

The above results indicate the effectiveness, both in terms of accuracy and stability, of this $\delta_0{}^2$ minimization method. It should be possible to achieve further improvements by changing the weight function $n(z)$ in the spacelike region and it is our intention to investigate this, as well as other variants of the general method.

ACKNOWLEDGMENT

Laboratoire de Physique Mathematique is Unité Associée No. 040768 au CNRS.

[1] J. S. Bell and R. A. Bertlmann, Nucl. Phys. **B187**, 285 (1981).

[2] J. Bowcock, S. Ciulli, and F. Geniet, Montpellier report (unpublished).

[3] L. J. Reinders, H. Rubinstein, and S. Yazaki, Phys. Rep. **127**, 1 (1985).

[4] For $v_0=10$ the integral over the branch cut, from s_0 to s_1, makes a contribution about $\frac{1}{10}$ of that due to the resonance; for $v_0=3$ the cut contribution is about $\frac{1}{4}$.

[5]The example to which Fig. 2 refers is described below in Sec. IV.

[6]M. Ciulli, S. Ciulli, and T. D. Spearman, J. Math. Phys. **25**, 3194 (1984); S. Ciulli and T. D. Spearman, Nuovo Cimento **83A**, 352 (1984).

[7]See Fig. 6 and the discussion of this in Sec. IV.

[8]N. Gorman, Ph.D. thesis, University of Dublin.

[9]A. Heyn and C. Lang, Z. Phys. C **7**, 169 (1981).

[10]S. R. Amendolia *et al.*, Nucl. Phys. **B277**, 168 (1986).

[11]The trial functions T_k were given the following form:

$$T_k(s)=-\left[\frac{\kappa}{\kappa+ik_0}\right]^2\left[\frac{\gamma\rho}{\kappa-(k_1+ik_2)}-\frac{(\gamma\rho)^*}{\kappa+(k_1-ik_2)}+c\right],$$

where $\kappa=\sqrt{s-s_0}$, and

$$\rho\equiv\frac{1}{\text{res}}=-\left[\frac{\kappa}{\kappa+ik_0}\right]^{-2}_{\kappa=k_1+ik_2}.$$

$T_k(s)$ as defined above has the required behavior at $s=s_0$, but is not zero at $s=0$. To obtain the zero value at $s=0$ one uses a subtracted form, $T_k(s)-T_k(0)$, for the trial function.

[12]The only restriction has been to take a real residue for the pole. This is certainly a reasonable assumption as in Sec. II the formula given in Ref. 11 has been used with $k_0=0$, $c=0$.